An experimental study on the data-driven structural health monitoring of large wind turbine blades using a single accelerometer and actuator.

David García[a,*], Dmitri Tcherniak[b]

[a] *University of Strathclyde, Mechanical and Aerospace Engineering, 75 Montrose Street, Glasgow G11XJ, United Kingdom*
[b] *Brüel & Kjær Sound & Vibration Measurement, Skodsborgvej 307, Nærum 2850, Denmark*

Abstract

The study aimed to investigate the performance of a Structural Health Monitoring (SHM) methodology based on use of a single accelerometer and single actuator in the detection and monitoring of the growth of the damage in the trailing edge of a wind turbine blade. The study used a data-driven vibration SHM, which is considered as a simple, nonparametric method for data compression and information extraction. The methodology found combinations of variables that describe major trends and fluctuations within the vibration response measured on the structure to create a reference state to which new observations were evaluated for damage diagnosis. The blade was artificially excited with an electromechanical actuator that introduced a mechanical impulse in the blade. The vibration responses were measured by accelerometers distributed along the trailing and leading edge of the wind turbine blade. The rationale behind this study was to investigate the combination of accelerometer/actuator location for damage detection sensitivity and damage progression when a single accelerometer and single actuator was used. The experimental study was conducted on an SSP 34 m wind turbine blade with and without introduced damage. Different damage sizes were also considered to evaluate the detectability of the damage. This study complements previous analyses in the same blade where studies on the effect of damage in modal parameters and a multiple sensor SHM technique were evaluated. The results demonstrated that the methodology was able to detect different damage sizes by using only one accelerometer. It was also demonstrated that damage detection and damage progression is affected by the accelerometer/actuator position but this effect is used to provide a rough information about damage location.

Keywords: data-driven techniques, singular spectrum analysis, wind turbine blade, structural health monitoring, damage blade assessment

1. Introduction

The current growth in the number of offshore wind turbines can be attributed to government's drive to reduce CO_2 emissions from energy production. Offshore wind energy production poses significant challenges but adds important green energy to the overall energy mix. Technological advances in this area could be

*Corresponding author
Email address: david.garcia@strath.ac.uk (David García)

hugely beneficial for securing the future of offshore wind energy. Presently, wind turbine blade maintenance involves visual inspection, which can be dangerous, time consuming and costly. Developing a remote blade condition monitoring system is therefore of great interest to the industry. Developing such a system would improve the operation and maintenance of the blades thereby reducing costs and helping to secure the future of clean energy [1]. There exist commercial condition monitoring systems for wind turbines. For example, companies Gram & Juhl and Brüel & Kjær Vibro GmbH provide solutions for condition monitoring of the drive trains and other mechanical components of wind turbines. Examples of commercially available SHM solutions are BLADEcontrol from Weidmüller Group, WindMETER from HBM, there are also solutions from Wölfel Engineering GmbH and Fos4x GmbH. These systems claim to be able to provide pitch control checks, condition monitoring, load assessment and ice detection, however, the publicly available sources do not provide information regarding the SHM capabilities of the systems nor any quantitative assessment of their damage detection statistics. The authors believe that further development of damage detection methodologies will enhance the already available condition monitoring solutions.

The idea of Vibration-based Structural Health Monitoring (VSHM) is a popular alternative, as vibration responses can be measured from a natural or artificial excitation in many available structures such as aircraft, railway vehicles, bridges, wind turbines with many others. The health/current state of the structure may be analysed by monitoring changes in its vibratory response. The monitoring process requires the observation of the system/structure over certain periods of time and this is the reason why an online monitoring procedure will benefit the maintenance process of remote structures such as offshore wind turbines. Farrar et al. [2] presented a monitoring procedure that is commonly used in the SHM community. The procedure is based on statistical pattern recognition and consists of four steps: (i) operation evaluation, (ii) data acquisition, (iii) feature extraction and (iv) decision making and classification. This monitoring procedure could successfully be implemented as a monitoring paradigm for the wind turbine blade. Each of these steps can be studied separately to fully accomplish the SHM philosophy and resolve some axioms presented by Worden et al. [3]. The axioms presented in the mentioned publication go from material damage identification to the evaluation of the trade-off between sensitivity to damage and noise rejection through intelligent feature selection. It is clear that some assumptions must be taken before each study or application to successfully obtain fruitful results depending on the goal of the analysis.

A common classification of VSHM methodologies is the division between model-based and non-model-based (or data-driven) methods. Model-based methods are commonly associated with the development of any analytical or numerical model which represents the structure in consideration. Experimental vibration responses are compared with the corresponding model in order to find similarities between the experimental and the simulated case. Model-based methods are generally used for model updating which uses experimental data to represent accurately the vibration behaviour of a real structure. One of the advantages of model-based methods is the use of an inverse problem that could well be extended to provide information about damage diagnosis as well as damage prognosis, which can predict, through simulation and past experience,

the remaining useful life of the system. An example can be found in [4] where the dynamic strain is predicted by a virtual sensing technique towards fatigue life monitoring.

Non-model-based methods rely purely on the data measured from the structure under study. These methods also involve a construction of a *model*, but this model is based on the data rather than numerical or analytical models [5]. The measurements in an early state of the structure are considered as the reference state, to which the measurements from the structure in operation will be compared. Any deviation of the new observations from the reference state may be considered as an indication of a damage. There are two main categories for these methods [6]: 1)*supervised*, when there is data available from both the healthy and the damaged structure and 2) *unsupervised*, when there is only data available from the healthy structure. Either method may be used depending on the data availability. In most cases, the data from the damaged structure is not available and therefore unsupervised methods are the ones with more interest. In practice most purely data-driven methodologies make use of data analysis techniques and utilise different statistical methods [7, 8]. Principal Component Analysis (PCA) is one such possibility and there are a number of publications that consider PCA-based damage assessment methods [9, 10] by considering both linear and nonlinear effects. In general, PCA is a technique used in data analysis to reduce the dimensionality of the available data. Since vibration signals in the time and/or a frequency domain have quite high dimension, it is obviously appropriate to apply such a technique to the measured vibration signals (see Jollife [11] for further information). PCA is useful for categorical data because it possesses a clustering effect in the sense that it reduces the distance between vectors from the same category, whilst at the same time, increases the distance between data vectors from different categories [12]. Some studies consider a PCA algorithm on parametric and nonparametric feature vectors (FV) to reduce the dimension of the FVs for damage detection as shown in [13] for the application of a lab-scale wind turbine blade with the consideration of different environmental conditions. In these studies, it can be observed the capability of PCA to compress and decompose the data in different principal components, which can be used in different manners with the aim of damage identification. The point is that PCA is generally developed for multiple and independent variables, while time series elements are usually non-independent, in the sense that they are related to each other and they should be considered as an entire measurement signal vector. This is one of the reasons why the methodology presented in this work uses the Singular Spectrum Analysis (SSA) technique, rather than PCA. This way, it takes care of the intercorrelation between the individual signal vectors obtained in the measured vibration responses. In this sense, SSA considers all the rotational patterns included in each vibratory signal rather than at a particular frequency. The aim of SSA is to decompose the original signal using a small number of independent, interpretable components which can be used for trend identification, detection of oscillatory components, periodicity extraction, signal smoothing, noise reduction and feature extraction [14]. Some studies have already used SSA-based methods for SHM as shown in [15] where SSA was applied for structural monitoring and damage diagnosis of bridges by using an eigenvalue ratio difference. Recently, SSA was used for the purpose of de-noising of the vibration responses measured on a machine

before subjecting the signal to autoregrasive modelling with application to fault detection in roller bearings [16]. A natural extension of SSA is Multichannel Singular Spectrum Analysis (MSSA). MSSA combines the ability of SSA to consider all rotational patterns in a single signal vector with the data compression properties of PCA to find common structure between the number of signal vectors considered. SSA can be applied in the time [17] and frequency domain [18]. This will depend on the aim of the study and therefore the interpretation of the results will be different [19]. Based on above introduction the work presented here introduces a VSHM methodology based on a data-driven technique with its foundations on SSA for wind turbine blade damage assessment.

The idea of develping an online remote system to monitor the health of wind turbine blades is of great interest. Vibration responses to either operational loads (operational modal analysis-based methods) or artificial induced excitation (actuator-based methods) are used as an input to statistical algorithms, which can detect and localize damage but also follow its growth. The system proposed in this work uses an electro-mechanical actuator medium frequency range excitation which is a good compromise between the wave propagation range and damage detection resolution. A similar actuator-based SHM system was successfully used for monitoring an operating Vestas V27 blade [20], and during a 3.5 months monitoring campaign, it had demonstrated an excellent robustness, despite the actuator being installed on the outer surface of the blade. For bigger blades, it is feasible to install the actuator inside the blade (as the actuator at location A3 in the present study, Fig.4(c)); installing it not further than 1/3 of the blade length from the blade root provides a sufficient signal-to-noise ratio for the measured acceleration signals even for the most remote points on the blade. As the actuator impacts the blade once every 5-10 minutes, its average energy consumption is quite modest. However, in any occasion, an SHM system design without the actuator is always an advantage, though it may demonstrate worse detection and false alarms rates. It is likely that advanced signal processing can, however, provide sufficient detection capabilities. Study [21] presents an example of successful detection without the use of the actuator based on the same data from the operating Vestas V27 wind turbine. As mentioned in [22], the range of frequencies employed in damage location has a great influence on the resolution of the results and also the physical range of application. The great advantage of using low frequency vibration measurements is that the low frequency modes are generally global and so the vibration sensors may be mounted remotely from the damage site. Equally, fewer sensors may be used. The problem with low frequency modes is that the spatial wavelengths of the modes are large, and typically are far larger than the extent of the damage [23]. Damage in the wind turbine blades first appears locally which is more difficult to detect. However, in the analysis of damage growth, it might have more global effects which contributes to its detection. This study is based on an experimental test of a 34 m wind turbine blade manufactured by SSP Technology A/S. The 34 m wind turbine blade has extensively been studied both experimentally [24] and numerically [25] at DTU Wind Energy. The effect of damage to the modal parameters [23] was investigated, and the study demonstrated that the natural frequencies are not a good indicator for damage detection. Mode shapes contain more information about the damage

where high modes shapes have higher sensitivity to damage. Other analysis was to study an unsupervised methodology that combines the correlation between signals measured from different accelerometers [26]. This study demonstrated that methodologies based on data-driven techniques have a lot of potential for damage detection in large structures such as SSP 34 m wind turbine blade. However, this study considered a minimum of five accelerometers to compute the damage indices. Therefore, a natural extension for the next study in this experimental test rig is presented in this manuscript. This study proposes a data-driven SHM methodology that considers the vibration responses measured by one sensor only. The rationale behind this work is to study the performance of the proposed methodology for investigating the one accelerometer/one actuator location towards minimising the equipment required and maximising the damage diagnosis.

The work presented in this manuscript is organised as follows; first the suggested methodology is introduced and tailored for wind turbine blade damage assessment. The experiment set-up along with the explanation of the artificial damage introduction and the data collection procedure is presented. The results are then investigated to offer discussion firstly, in the considerations and the effect of selecting the number of features. Secondly, in the performance of the proposed VSHM methodology for both the damage detection and the damage progression at different actuator and accelerometer locations. Finally the conclusions of the study are presented to define the limitations of the study and future research ideas.

2. Methodology for damage assessment in wind turbine blades

The methodology presented in this study is considered as a simple nonparametric method for data compression and information extraction, which finds combinations of variables that describe major trends and oscillations in the vibratory signals measured on the structure/system in consideration [27]. The procedure is divided into four steps: data collection, creation of the reference state, feature extraction and inspection phase for decision making [28].

2.1. Data collection

The first step is to collect the data from the structure/system in consideration that particularly in this study is a wind turbine blade as presented and defined in section 3. Acceleration signals are measured and discretised into a vector with $\bar{N}$ time sampling points. Each measured signal is first standardised to have zero mean and unit variance, and secondly transformed to the frequency domain to obtain signal vectors $\mathbf{x}_m$ with length $N = \bar{N}/2$ where $m = 1, ..., M$ is the number of signal vector realisations measured as shown in Eq. 1 where the superscript t symbolises transpose.

$$\mathbf{x}_m = (x_{1,m}, x_{2,m}, ..., x_{N,m})^t \tag{1}$$

Each signal vector realisation is arranged in the columns of the matrix $\mathbf{X}$ with dimension $[N \times M]$ as

shown in Eq. 2.

$$\mathbf{X} = (\mathbf{x}_1, \mathbf{x}_2, ..., \mathbf{x}_M) \tag{2}$$

The matrix $\mathbf{X}$ is constructed from signal vectors obtained on the pristine/healthy state of the wind turbine blade and it is used for creating the reference state as explained in the next section.

2.2. Creation of the reference state

A reference state is created based on the matrix $\mathbf{X}$ where the observation signal vectors can be compared. The steps for creating the reference state are the following: embedding, decomposition and reconstruction. These steps are explained as follows.

2.2.1. Embedding

This step creates an embedding matrix of each signal vector contained in $\mathbf{X}$. By creating an embedding space, more dimensions are introduced and thus more features of the signal vector are uncovered. In this sense, each vector signal $\mathbf{x}_m$ is embedded into a matrix $\check{\mathbf{X}}_m$ by W-lagged copies of itself as shown in Eq. 3 where $m = 1, ..., M$ and W are the number of signal vector realisations and the sliding window size, respectively. The dimension of the matrix $\check{\mathbf{X}}_m$ is $[N \times W]$.

$$\check{\mathbf{X}}_m = \begin{pmatrix} x_{1,m} & x_{2,m} & x_{3,m} & \cdots & x_{W,m} \\ x_{2,m} & x_{3,m} & x_{4,m} & \cdots & x_{(W+1),m} \\ x_{3,m} & x_{4,m} & x_{5,m} & \cdots & \vdots \\ x_{4,m} & x_{5,m} & \vdots & \cdots & \vdots \\ x_{5,m} & \vdots & \vdots & \cdots & x_{N,m} \\ \vdots & \vdots & x_{(N-1),m} & \cdots & 0 \\ \vdots & x_{(N-1),m} & x_{N,m} & \cdots & 0 \\ x_{(N-1),m} & x_{N,m} & 0 & \cdots & 0 \\ x_{N,m} & 0 & 0 & \cdots & 0 \end{pmatrix} \tag{3}$$

The embedding process defined in Eq. 3 is applied to each vector signal realisation as mentioned above. All matrices $\check{\mathbf{X}}_m$ are used to create the full embedded matrix $\check{\mathbf{X}}$. The dimension of the full embedded matrix $\check{\mathbf{X}}$ detailed in Eq. 4 is $[N \times (MW)]$. The number of M-signal vector realisations and the W sliding window size considered in the full embedded matrix $\check{\mathbf{X}}$ are selected so that $M \leq W$ and $W \leq N/2$.

$$\check{\mathbf{X}} = (\check{\mathbf{X}}_1, \check{\mathbf{X}}_2, ..., \check{\mathbf{X}}_M) \tag{4}$$

2.2.2. Decomposition into Principal Components

The full embedding matrix $\check{\mathbf{X}}$ defined in Eq. 4 is decomposed into a number of vector components based on their variance content within the vibration response. First, the covariance matrix of $\check{\mathbf{X}}$ is calculated as

detailed in Eq. 5.

$$\mathbf{C}_X = \frac{\check{\mathbf{X}}^t \check{\mathbf{X}}}{N} \tag{5}$$

The matrix $\mathbf{C}_X$ defines the covariance between the different signal vector realisations and has a dimension $[(MW) \times (MW)]$. In Eq. 5, $\check{\mathbf{X}}$ is the full embedding matrix, $\check{\mathbf{X}}^t$ is the transpose matrix of $\check{\mathbf{X}}$ and N is the signal vector dimension. As the covariance matrix is calculated on the full embedding matrix, not only the auto-covariance of each signal vector realisation is considered but also the cross-covariance between the signal vector realisations is also taken in to account.

The eigendecomposition of $\mathbf{C}_X$, defined in Eq. 6, yields λ_k eigenvalues stored in the diagonal matrix $\mathbf{\Lambda}_X$ in decreasing order and $\mathbf{E}^k$ eigenvectors stored in columns into the matrix $\mathbf{E}_X$ in the same order as their corresponding eigenvalues. Each eigenvalue defines the partial variance in the direction of its corresponding eigenvector, therefore the sum of all eigenvalues gives the total variance of $\mathbf{X}$.

$$\mathbf{E}_X^t \mathbf{C}_X \mathbf{E}_X = \mathbf{\Lambda}_X \tag{6}$$

The matrix $\mathbf{E}_X$ contains all eigenvectors $\mathbf{E}^k$ with dimension $\{\mathbf{E}^k : 1 < k \leq MW\}$. Each eigenvector $\mathbf{E}^k$ is composed of M consecutive on length W, depending on the number of signal vector realisations and sliding window size, respectively, with its elements denoted as $E^k_{m,w}$. Each Principal Component (PC) $\mathbf{A}^k$ associated with each eigenvector $\mathbf{E}^k$ is calculated by projecting the matrix $\check{\mathbf{X}}$ onto $\mathbf{E}_X$ as shown in Eq. 7 where $n = 1, ..., N$ (see [27]).

$$\mathbf{A} = \check{\mathbf{X}} \mathbf{E}_X \tag{7}$$

Therefore, each PC contains characteristics from all the M signal vector realisations.

2.2.3. Reconstruction of the reference state

This section explains how to obtain the Reconstructed Components (RCs) which are linear combinations of the PCs and the eigenvectors. The RCs are calculated by convolving the PCs with the associated $\mathbf{E}^k$, thus the k^{th} RC at n-value and m-realisation is given by Eq. 8.

$$R^k_{m,n} = \frac{1}{W_n} \sum_{w=1}^{W} A^k_{n-w+1} E^k_{m,w} \tag{8}$$

Each $R^k_{m,n}$ value is normalised by the normalisation factor W_n which is described by the Eq. 9.

$$W_n = \begin{cases} n & 1 \leq n \leq W-1 \\ W & W \leq n \leq N \end{cases} \tag{9}$$

The RCs are then arranged in columns into the matrix $\mathbf{R}$ with a dimension $[N \times (MW)]$. Therefore, $\mathbf{R}$ can be used as the reference state of the structure/system to which the observation signal vectors are compared.

2.3. Feature extraction

A Feature Vector (FV) is obtained for each new observation signal vector which will be subjected to damage evaluation by comparing its similarity to the reference state defined by $\mathbf{R}$. Therefore, an FV is calculated by multiplying an observation signal vector $\mathbf{x}$ with each RC in the reference state $\mathbf{R}$ as shown in Eq. 10 where $j = 1, ..., W$.

$$T_j = \sum_{n=1}^{N} x_n R_{n,j} \tag{10}$$

Each T_j value represents the inner product between an observation signal vector and each RC. All T_j are arranged into a vector $\mathbf{T}$ with dimension W. The FV $\mathbf{T}$ characterises the observation signal vector onto the feature space.

2.4. Inspection phase and decision making

2.4.1. Damage assessment index

This section presents how damage is evaluated from the FVs defined in section 2.3. First, the baseline feature matrix $\mathbf{T}_B$ is created with a dimension $[p \times s]$ where p is the dimension selected from the FV $\{\mathbf{T} : p \leq W\}$ and s is the number of signal vectors utilised to define the baseline matrix as shown in Eq. 11.

$$\mathbf{T}_B = \begin{pmatrix} T_{1,1} & T_{2,1} & \cdots & T_{p,1} \\ T_{1,2} & T_{2,2} & \cdots & T_{p,2} \\ \vdots & \vdots & \cdots & \vdots \\ T_{1,s} & T_{2,s} & \cdots & T_{p,s} \end{pmatrix} \tag{11}$$

Once the baseline is defined, an observation FV is then compared with the baseline $\mathbf{T}_B$. Each observation FV has to have the same dimension p as the baseline and is defined by $\mathbf{T}^i = (T_{1,i}, T_{2,i}, ..., T_{p,i})$ where i is the number of observation FVs.

The next step is to measure the similarity of an observation FV $\mathbf{T}^i$ to the baseline feature matrix $\mathbf{T}_B$. To demonstrate this, an outlier analysis using the Mahalanobis distance is carried out on the observation FVs. An outlier analysis calculates a measure of how similar or dissimilar an observation FV is to the baseline. The measured discordance is calculated as shown in Eq. 12 where $\boldsymbol{\mu}_B$ is the mean row of the baseline feature matrix $\mathbf{T}_B$, $\boldsymbol{\Sigma}$ is its corresponding covariance matrix and D_i is the damage index.

$$D_i = \sqrt{(\mathbf{T}^i - \boldsymbol{\mu}_B)^t \boldsymbol{\Sigma}^{-1} (\mathbf{T}^i - \boldsymbol{\mu}_B)} \tag{12}$$

2.4.2. Threshold setting for inspection phase

In order to label an observation as an outlier or inlier there is a need to define a threshold to which the damage indices can be evaluated.

A probabilistic threshold D_T based on the probability density function (pdf) of the distances measured by the baseline FVs to the baseline matrix $\mathbf{T}_B$ is calculated. The damage indices are always positive ($D > 0$). Based on this assumption, a log-normal probability density function is used to approximately fit the data considered as training set (observations from the healthy wind turbine blade), in order to set a threshold to distinguish between observations from healthy and damaged structure. This kind of damage classification, using a probability test, was also studied in [29] where different probability distributions were considered. A lognormal probability density function is described by Eq. 13.

$$f(D|\mu,\sigma) = \frac{1}{D\sigma\sqrt{2\pi}} exp\left[\frac{-(lnD-\mu)^2}{2\sigma^2}\right] \quad ; \quad D > 0 \tag{13}$$

where:

D: Damage indices obtained by observations of the healthy blade considered as training data set

$ln\ D$: is the natural logarithm of D

μ, σ: are mean and standard deviations of $ln\ D$, respectively

Then, the threshold D_T is selected by a particular risk level which determinates the false alarm probability equal to α in the lognormal density function as shown in Fig. 1(a) . The threshold is calculated by the inverse of the lognormal cumulative density function which gives the value with probability $1-\alpha$ in the cumulative density function, described by Eq. 14 (see Fig. 1(b)).

$$D_T = F^{-1}(pn|\mu,\sigma) = \{D_T : F(D|\mu,\sigma) = pn\} \tag{14}$$

$$pn = F(D|\mu,\sigma) = \frac{1}{2}\left[1 + erf\left(\frac{lnD-\mu}{\sigma\sqrt{2}}\right)\right] \tag{15}$$

where:

pn: is the lognormal cumulative density function described by Eq. 15

erf: is the error function defined as $erf(D) = \frac{2}{\sqrt{\pi}}\int_0^D e^{-t^2}dt$ (see [30] p.110)

D_T: is the value of the sampling training data with probability $1-\alpha$ selected to be the threshold

Therefore, any observation damage index D_i in the range [0, D_T] will be considered as an observation from the healthy wind turbine blade and anything else will be considered as a damaged wind turbine blade as described by the following decision rules.

$$\begin{aligned} &\mathbf{H_0}: \quad D_i \leq D_T \quad \Rightarrow \quad \text{Undamage wind turbine blade} \\ &\mathbf{H_1}: \quad \text{Else} \quad \Rightarrow \quad \text{Damaged wind turbine blade} \end{aligned} \tag{16}$$

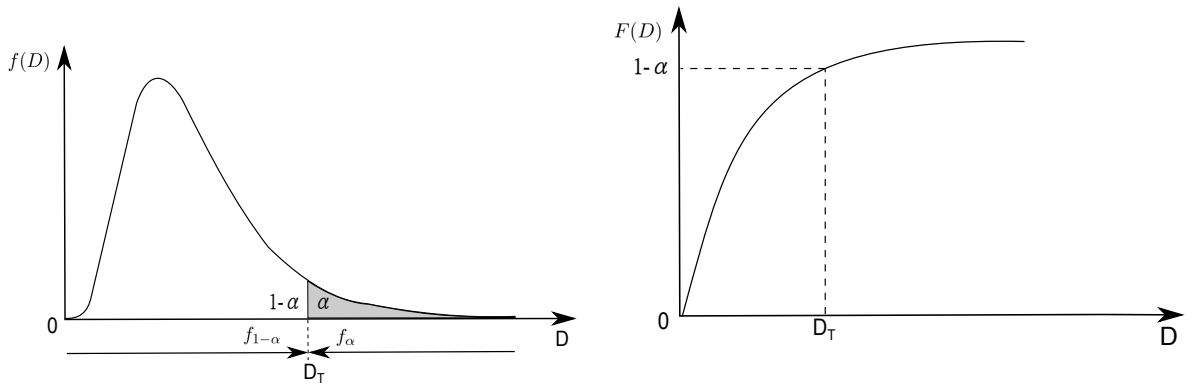

(a) (b)

Figure 1: Statistical hypothesis threshold based on lognormal distribution (one-side only). a) Probability density distribution. b) Cumulative density function.

3. Experiment set-up

3.1. Test rig

The SSP 34 m blade is a 34 meters wind turbine blade manufactured by SSP-Technology A/S. The blade was mounted on a test rig in the indoor test facilities of the Wind Energy department (formerly Risø) the Technical University of Denmark, the set-up is shown in Fig. 2(b). The detailed description of the test rig and the blade can be found in [31].

The blade was instrumented with 20 triaxial accelerometers, Brüel & Kjær Type 4524-B, 10 along the Leading Edge (LE) and 10 along the Trailing Edge (TE) as shown in the scheme in Fig. 2(a). Only the acceleration in the direction normal to the blade surface, which coincides with the flap-wise motion of the blade, was utilized. The overview of the sensors placement and their orientation is shown in Figure 3 in [23]. The acceleration signals were recorded by a distributed data acquisition system based on several 12 channel data acquisition modules Brüel & Kjær Type Type 3053-B and data recording software Brüel & Kjær Type Type 7708. The detailed description of the measurement set-up can be found in [23].

The VSHM methodology conducted in this study is based on active excitation system; four electromechanical actuators (Fig. 2(c)) were installed on the blade. The actuator consists of three main parts: a steel plunger with a hard plastic tip, the coil and the base. When an electrical pulse is driven through the coil, it applies an impulse to the plunger, which impacts the structure; after the hit, the plunger retracts to its initial position by a spring and stays there until the next electrical pulse is transferred to the coil. The detailed description of the actuator is provided in [26].

3.2. Artificial damage simulation

One of the most common types of damage of this kind of blades is when the adhesive bond between the laminates of the pressure and suction sides of the blade breaks; this can happen on both leading and trailing

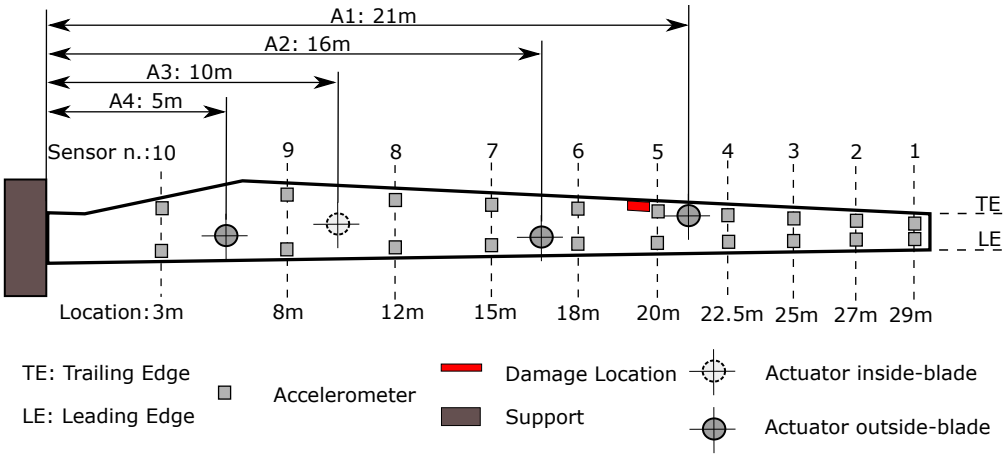

(a)

(b)

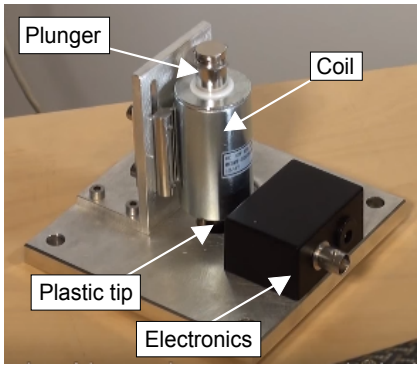

(c)

Figure 2: Experiment set up of the SSP 34 m wind turbine blade. a) Accelerometers, damage and actuators locations scheme. b) Test rig set-up. c) Electromechanical actuator.

edges of the blade. Due to the stress concentration around the damaged region, especially near the tip and the max chord region, a small failure can grow to a level at which repair is impossible, and the entire blade should be replaced.

A similar failure was introduced artificially into the trailing edge of the blade. First, a series of holes through the adhesive between the pressure and suction sides of the blade were drilled. Then, using a saw and a chisel, the holes were merged together, forming an opening that was gradually extended from 20 cm up to 120 cm by increments of 20 cm as shown in Fig. 3(a).

The use of heavy hammer and chisel could introduce some other unwanted changes into the blade and the measurement set-up. The following was done to ensure that the change in vibration pattern is exclusively due to the introduced structural damage: the debonded parts were connected by bolts, placed at 10 cm intervals. The glue removed between the shells was replaced by thin metal plates as shown in Fig. 3(b). Then the healthy blade was modelled by tightening all the bolts; the damaged blade was simulated by loosening some bolts, where the amount of damage could be defined by the number of the loosened bolts. The bolts and

the metal plates were not removed from the blade opening in order to keep the local mass constant. Failures with different severities were introduced as described in Table 1; this was done to simulate different damage locations and damage progression.

(a) (b)

Figure 3: Damage introduced in SSP 34 m wind turbine blade. a) Damage introduced by chisel in the trailing edge. b) Damage bolted to control the damage size and any additional anomalies introduced by the impact that generates the damage

(a) Actuator location A1 (b) Actuator location A2 (c) Actuator location A3 (d) Actuator location A4

Figure 4: Actuator locations on the SSP 34 m wind turbine blade

3.3. Data collection procedure

The nature of the presented algorithm requires the data from the undamaged blade to create the reference state to act as a baseline for the observations that follow. Since the experimental data is always contaminated by noise, it is useful to repeat the measurements several times. Table 1 details the number of measurements for each blade state with a total of 386 measurements per accelerometer, for each of the four actuator locations. To accelerate the test, the time between the successive actuator impacts was set varying from one to five minutes. However, in real-life applications, the time between the measurements can be extended to one hour or more depending on the industrial requirements.

The actuator locations are detailed in Fig. 2(a). Actuator A1 was located very close to the accelerometer 5 in the trailing edge; this is the closest actuator to the damage (see Fig. 4(a)). Actuator A2 was placed close to the leading edge between accelerometers 6-7, see Fig. 4(b). Actuator A3 is the only one mounted inside the blade, specifically, inside the spar beam. It was placed between accelerometers 8-9 approximately in the

Table 1: Number of signals measured on each experimental test

Scenario	Damage	Designation	Number of Signals
Undamaged blade	–	H	53
Training	–	–	26
Testing	–	–	27
Damaged blade	20 cm	D20	70
	40 cm	D40	61
	60 cm	D60	60
	80 cm	D80	49
	100 cm	D100	54
	120 cm	D120	39
TOTAL			386

middle between the webs connecting the suction and pressure sides of the blade (see Fig. 4(c)). Finally, actuator A4 was placed very close to the root of the blade, between accelerometers 9-10. This is the farthest actuator from the damage (see Fig. 4(d)).

The data collection procedure was implemented as follows: 1) All bolts were tightened (to represent the undamaged state of the blade) and all 20 acceleration signals were measured when the blade was excited by the actuator A1. After few seconds delay ensuring the response from the impact has decayed, the blade was excited by the actuator A2, then, similarly, by the A3 and the A4. 2) Once the set of accelerations responses of the undamaged blade was finished, the first damaged scenario (20 cm opening, state D20) was introduced by loosening the designated bolts and the series of measurements was repeated. 3) Then more bolts were loosened to introduce a 40 cm opening (state D40), and a series of the measurements were repeated. The same procedure was repeated for damaged states D60, D80, D100 and D120 (see Table 1).

4. Results and discussions

This section presents the main results and discussions of the methodology performance applied to the SPP 34 m wind turbine blade. First, the results obtained by exciting the wind turbine blade in the location A1 were selected to study and gain knowledge about the methodology and its performance when different FV dimensions were considered. Secondly, the study of the performance of the methodology by exciting the wind turbine blade at the different locations and comparing the different accelerometer/actuator locations for the damage detection sensitivity and the damage progression.

4.1. Study and performance of the methodology

The methodology described above was first applied when the wind turbine blade was excited in the actuator location A1 and the acceleration responses were measured by the accelerometer 1 in the trailing edge (see Fig. 2(a) for the actuator and the accelerometer location). The reference state was created by the free-decay acceleration responses sampled at 16384 Hz measured by the same accelerometer when the blade was undamaged. As mentioned in the introduction, the data from the SSP 34 m blade tests was used

for different analysis and therefore the vibration responses were intentionally recorded with high sampling frequency. For this methodology, it would not be necessary to have such a high sampling frequency but as the signals were measured with these characteristics, they were used as such. The performance of the methodology has demonstrated successful results for this high sampling frequency as it was able to smooth the frequency responses for better damage diagnosis. On the other hand, a prior knowledge about the vibrations caused by the actuator and the operational vibrations caused by wind may benefit the results. This can be observed in [32], where a band-pass filter was applied in order to ensure that the most informative frequency range is used in damage detection, thus the less informative low frequencies (damage-insensitive) and high frequencies (low energy) are excluded from the consideration. From the vibration responses measured on the undamaged blade, $M = 10$ signal vector realisations with a sliding window size $W = 10$ were selected to create the reference state. The selection of the sliding window size W will affect the signal decomposition in the SSA methodology and it will depend on each case of study. A study was presented in the effect of W when SSA is applied in the time domain or frequency domain [19]. As a general overview, when, it comes to the frequency domain, a large number of W will result in an excessively smooth version of the original signal and therefore the consideration of more RCs will be needed to represent the dynamics of the measurement. However, a relatively small number of W will provide a smoother version of the original signal that generally provide good performance of the methodology by considering small number of RCs. The selection of this value will affect to the number of RCs selected to obtain the damage indices. As mentioned in section 2.2.1, the number of M-signal vector realisations and the W sliding window size considered in the full embedded matrix $\check{\mathbf{X}}$ are selected so that $M \leq W$ and $W \leq N/2$. The vibration responses were transformed to the magnitude frequency domain by the Fourier transform, and then discretised into vectors of length $N = 2048$. With these signal vectors, the embedding matrix $\check{\mathbf{X}}$ had a dimension $[2048 \times 100]$. The eigendecomposition of covariance matrix of the embedding matrix yields to a total of 100 eigenvalues and their corresponding eigenvectors. Therefore, the reference state $\mathbf{R}$ created through the methodology had a dimension $[2048 \times 100]$.

Fig. 5(a) shows the eigenvalue spectra in decreasing order of the first 20 eigenvalues. In Fig. 5(a), it can be observed that the first three eigenvalues, and hence their corresponding eigenvectors, contain the majority of the variability of the signal vectors and therefore they will contribute more towards the signal reconstruction. Fig. 5(b) shows the comparison between the original frequency spectrum and the reconstructed frequency spectrum for 2 RCs and 5 RCs. It can be observed that the reconstruction with 2 RCs is smoother than the reconstruction with 5 RCs. Therefore, it is clear that depending on how many RCs are used to obtain the FVs, more or less information in the original spectral line will be taken into account [19].

The FVs were obtained by projecting the observation FVs onto the reference state as explained in section 2.3. In order to compare the effect of the FVs' dimension in the performance of the methodology, different values of $p = 2, 3, 4, 5$ and 6 were considered separately. All observation FVs were projected onto the p-dimensional feature space where they are now represented by means of the reference state. A number of FVs measured on the undamaged blade were considered as training data to create the baseline matrix where the

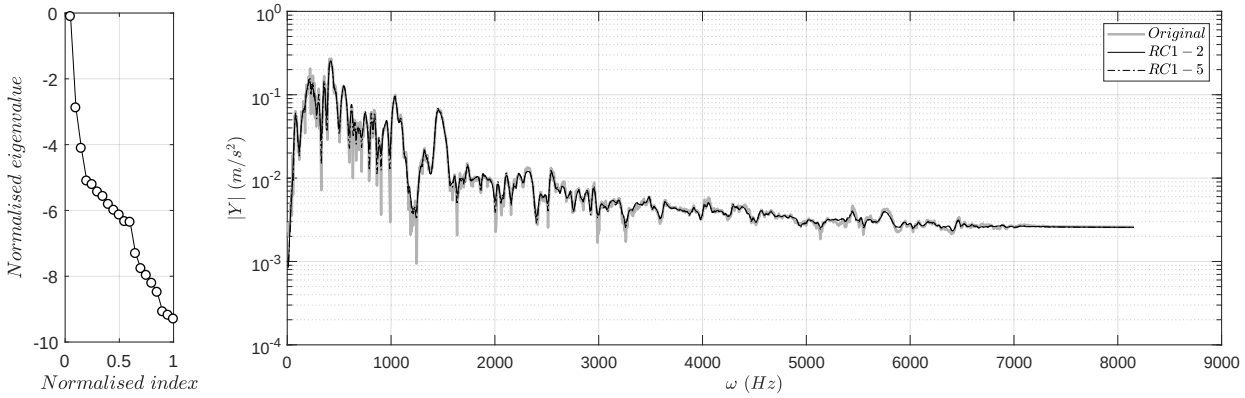

(a) (b)

Figure 5: Example of decomposition and reconstruction of a signal measured on the undamaged blade by accelerometer 1 in the trailing edge by the actuation in location A1. a) Normalised eigenvalue spectra of the first 20 eigenvalues. b) Comparison of the original and the reconstructed spectrum by 2 RCs and 5 RCs.

observation FVs can be compared. Therefore, the baseline matrix $\mathbf{T}_B$ was constructed by $s = 26$ FVs with a dimension p as defined above. The Mahalanobis distance of each observation to the baseline matrix was measured to determine the damage index of each observation. A threshold was found based on the damage indices of the observation points of the undamaged blade considered as training data records ($s = 26$) to the baseline matrix $\mathbf{T}_B$. The threshold was found as explained in section 2.4.2 with a risk of false alarm probability equal to $\alpha = 0.01$. In Fig. 6, it can be observed a good fit of the reference data and the selected probability distribution.

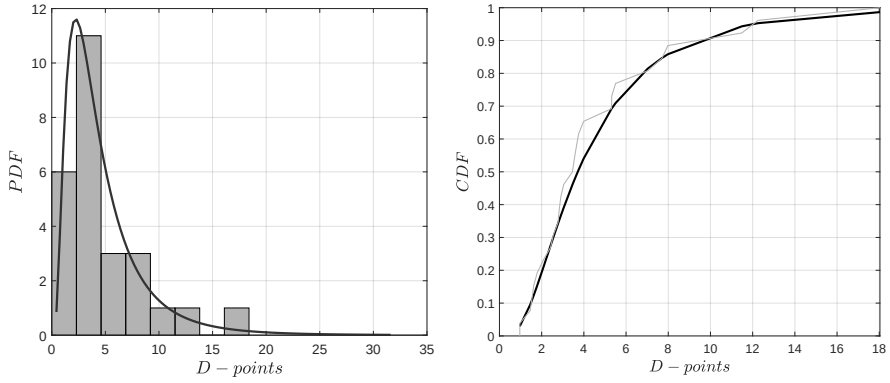

(a) (b)

Figure 6: Statistical hypothesis threshold based on lognormal distribution (one-side only) for signals measured by accelerometer 1 in the trailing edge for the actuation in the location A1. a) Probability density distribution. b) Cumulative density function.

As a visualization of the methodology performance, the damage indices obtained by accelerometer 1 at the TE are presented in Fig. 7 for an FV dimension $p = 2$ and $p = 5$. It can be observed that by considering

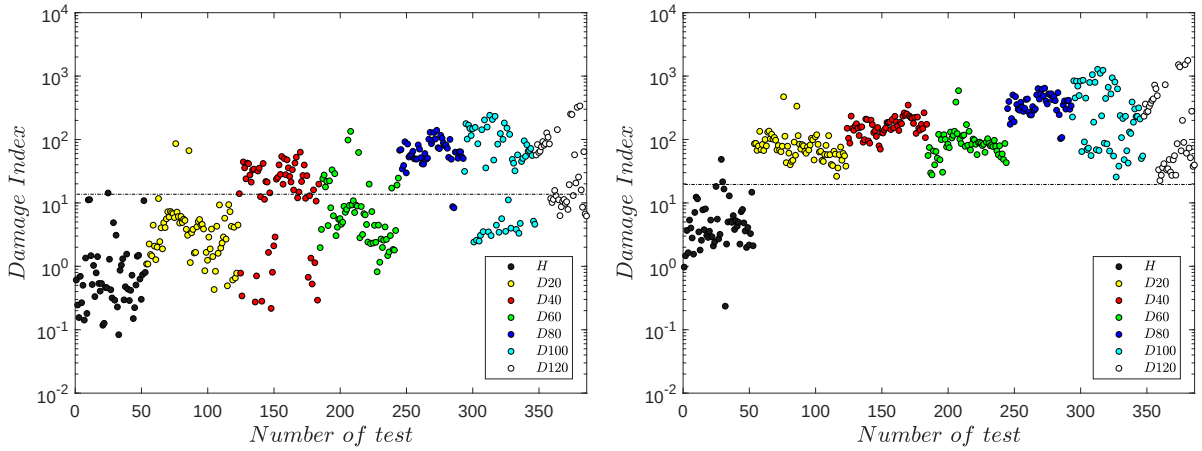

(a) (b)

Figure 7: Mahalanobis based damage index of measurements obtained in the accelerometer 1 in the trailing edge by the actuation at location A1. a) FV - Dimension $p = 2$ and b) FV - Dimension $p = 5$. The dashed line is the threshold calculated by a risk of false alarm probability equal to $\alpha = 0.01$.

an FV with dimension $p = 2$, the detection of the damage was not successfully achieved for the majority of the observations. The observations from the wind turbine blade with damage size 20 cm was not detected. Although the damage indices slightly increased with the damage size, the majority of observations were below the defined threshold. However, when the FV dimension was increased up to $p = 5$, all the observations measured in a damaged blade were detected as such. On the other hand, the number of observations from the undamaged blade led to damage indices above the defined threshold (false positives) and therefore this reduces the reliability of the damage assessment.

The performance of the methodology was studied for all the accelerometers along the trailing edge when the excitation on the blade was again executed in the location A1. The analysis presented here was to compare the classification rate, the percentage of true negatives and true positives, of the different undamaged and damaged scenarios (see Table 1) by each accelerometer in the trailing edge and for all different different p-dimensions defined above. The reason for this analysis was to easily visualise the damage detection performance of the methodology for a fixed accelerometer and fixed actuator location to understand the influence of the FV dimension for the damage assessment.

Fig. 8 represents the classification rates by means of the percentage of the true negatives on the top row designated by H (i.e. how many data records measured in the undamaged blade were classified as such). The following rows indicate the percentage of the true positives designated by D# depending on the damage size as detailed in Table 1 (i.e. how many data records measured in a damaged blade D# were classified as such). Colours represent the percentages from white (100% correct classification) to black (0%). This classification rate was calculated for different p-dimensions of the FVs considered in the methodology for a threshold with risk $\alpha = 0.01$. In order to clarify the analysis, it is needed to mention that the reference state was calculated independently for each accelerometer location, therefore the analysis was done for a

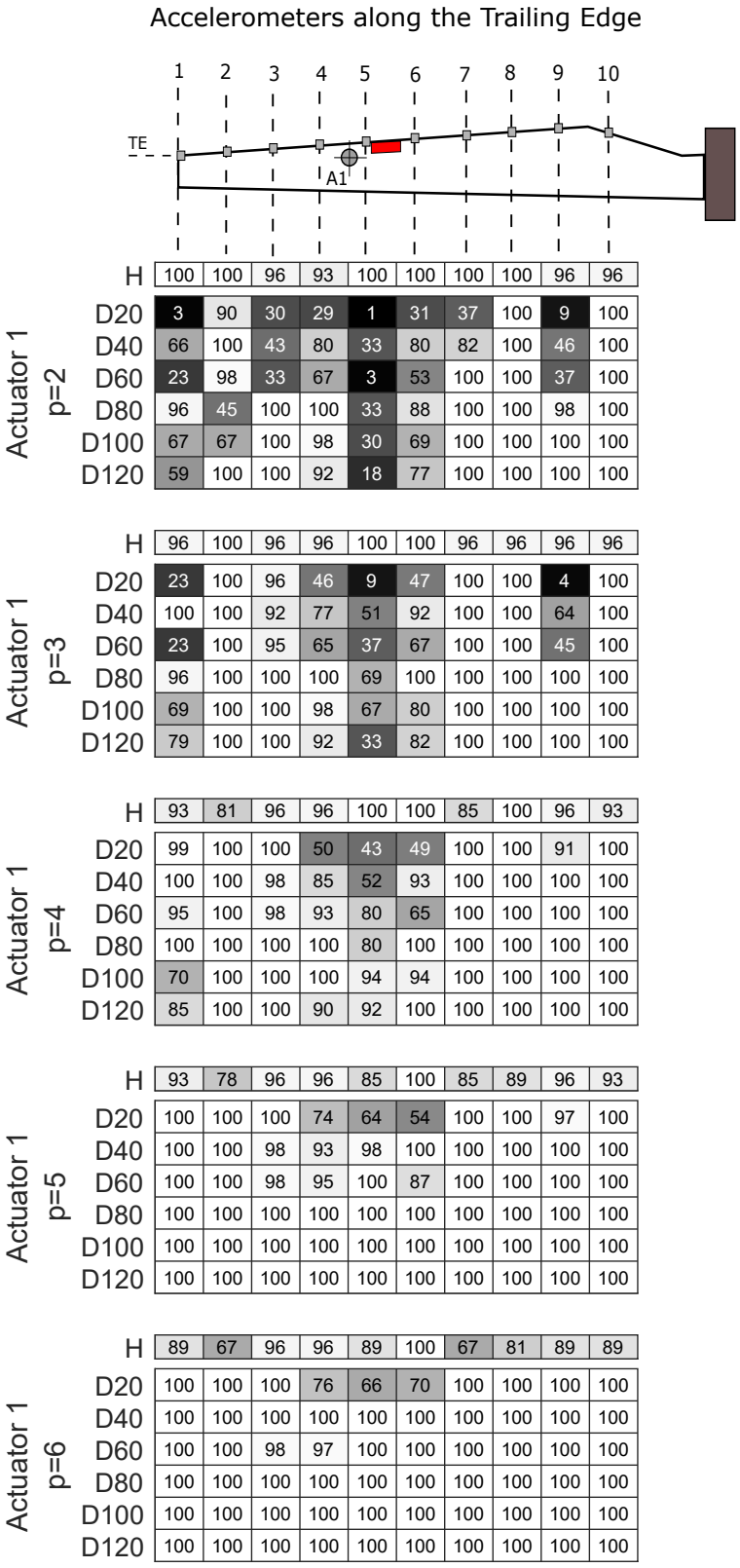

Figure 8: Percentage of correct classification rates for undamaged and different damaged observations (true negatives and true positives) in the accelerometers along the trailing edge by the actuation in A1 for different dimensions of the FV. The threshold at risk of false alarm probability equal to $\alpha = 0.01$. The number of observations for each scenario are defined in Table 1.

single accelerometer each time. $M = 10$ signal vector realisations were used from each sensor to build the reference sate and therefore the FVs of each accelerometer were calculated by means of its corresponding reference state. Also the threshold setting varied for each accelerometer as the distribution of the training data records was slightly different in each case but they follow a similar distribution to the one presented in Fig. 6. Then, the observation FVs were projected onto their corresponding p-dimensional feature space and finally the damage indices were calculated.

The performance of the methodology can be seen in Fig.8 where the percentage of true negatives and true positives is displayed for the case of the excitation at location A1 and for the accelerometer 1 in the trailing edge. It can be seen that for a low number of RCs ($p = 2$), the true negatives rate is high, but this also implies a small percentage of the true positives for the majority of the accelerometer locations. On the other hand, it can be observed that, by increasing the number of RCs ($p = 3$, 4, 5, 6), the percentage of true positives increases but this negatively affects the percentage of true negatives. This allows us to suggest that retaining more RCs in the feature space provides higher percentage of the true positives but it will negatively affect to the true negatives. However, it can be observed that for $p = 6$ RCs, the percentage of true positives does not increase significantly but it does affect to the percentage of true negatives. This demonstrates the statement that any information retained after the eigenvalue spectra graph changes the slope, which occurs between the eigenvalue 4 and 5 as shown in Fig. 5(a), will not add valuable information in the RCs and therefore it will affect negatively to the classification rates. This is a subjective procedure of selecting the number of components based on the slope of the eigenvalue spectra as discussed in [11] (page 115) and applied in [33]. This approach has been used to select the dimension of the feature space for the comparison of the methodology performance for the different actuation locations on the blade. It can be observed in 5(b) that the reconstructions with 2 or 5 RCs are very similar. However, in Fig. 7, it is observed that the consideration of 5 RCs in the feature space provides 100% of true positives with reasonable low number of false positives meanwhile the use of only 2 RCs does not provide a high percentage of true positives for any of the damage sizes, or in other words, bad damage detection.

4.2. Damage assessment by comparing different actuator locations

The results presented in this section are based on the study of the performance of the methodology for a fixed damage location and a defined set of damage sizes when the wind turbine blade was excited independently at each location A1, A2, A3 and A4. As explained in section 3.3, the main goal of this study was to investigate the damage detection performance for different actuator and accelerometer locations. The best SHM methodology should have a classification of 100% true negatives and 100% true positives. However due to several reasons, it is difficult to achieve these classification rates. Therefore, the main role of a SHM methodology is to separate and/or clearly distinguish between observations from undamaged blade and damaged blade in order to set a reliable threshold to make the decision whether a new observation is undamaged or damaged. In this study, the threshold has been set up by selecting a risk false alarm probability based on the probability density function of the training data set. Then, the new observations

are compared to this threshold and the classification rate is calculated. The main goal of this study was to compare for the same parameters (i.e. same number of RCs for building the feature space, same number of training data set, same threshold and same number of observations) to the performance of a data-driven SHM methodology when the measurements are considered from a single accelerometer. Thus, the location of the accelerometer in relation to the damage location will not only contribute towards the damage detection but also to estimate roughly the damage localisation by evaluation the performance of the methodology in each accelerometer separately. Similarly than in the previous section, $M = 10$ signal vectors and sliding window size of $W = 10$ were used for constructing the references state. The FV dimension selected for the analysis was $p = 5$ as discussed and concluded in section 4.1. For all the cases, the eigenvalue spectra changed its slope before the 5^{th} eigenvalue and thus this was the assumption for selecting the FV dimension. The number of measurements considered for the evaluation of performance of the methodology are presented in Table 1. Fig. 9 contains the results of the percent of correct classification (true negatives and true positives) for undamaged and damaged blade when measured at each accelerometer of the trailing and leading edge by exciting at each of the different actuator locations. As a first observation, it was clearly observed that the accelerometers along the TE detected the damage better than the accelerometers along the LE. Evaluating the performance of the methodology for each accelerometer in the TE, it can be observed that the location of the actuator plays an important role. When the excitation was performed on the actuator location A1 and A2, which are the closest to the damage and to the tip of the blade, the percentage of true negatives and true positives was high for the majority of the accelerometers along the trailing edge. However, for the actuator locations A3 and A4, the rates of the true negatives and true positives decreased significantly, which made the damage detection poor for some accelerometer locations. The actuator at A3 provided significantly low percentage of true negatives and true positives compared to the other actuator locations. Only accelerometers behind the damage towards the tip on the TE provided high percentage of true positives with reasonable percentage of true negatives (i.e. accelerometers 1, 2, 3). This phenomenon aligns with the outcomes in [25] where the elastic waves were simulated when the actuation was in A3. It was observed that the elastic waves travelled along the spar beam of the blade until they interacted with the damage region to further continue towards the tip of the blade. For this reason, the accelerometers behind the damage towards the tip gave higher percentage of true positives in comparison with other accelerometers. In addition, based on the comparison of methodology's performance for all the accelerometer locations (leading and trailing edges), a rough information about the damage location can be obtained. The highest percentage of true negatives and true positives was achieved by the accelerometers in the trailing edge. This shows that damage in the edges of the blade presents a local effect over the entire blade.

4.3. Damage progression

Generally, detecting damage by a data-driven SHM methodology will require monitoring a feature that provides information about the current status of the structure, the wind turbine blade in this study. Sometimes, as discussed in the previous section, the selected feature does not always provide a clear indication of

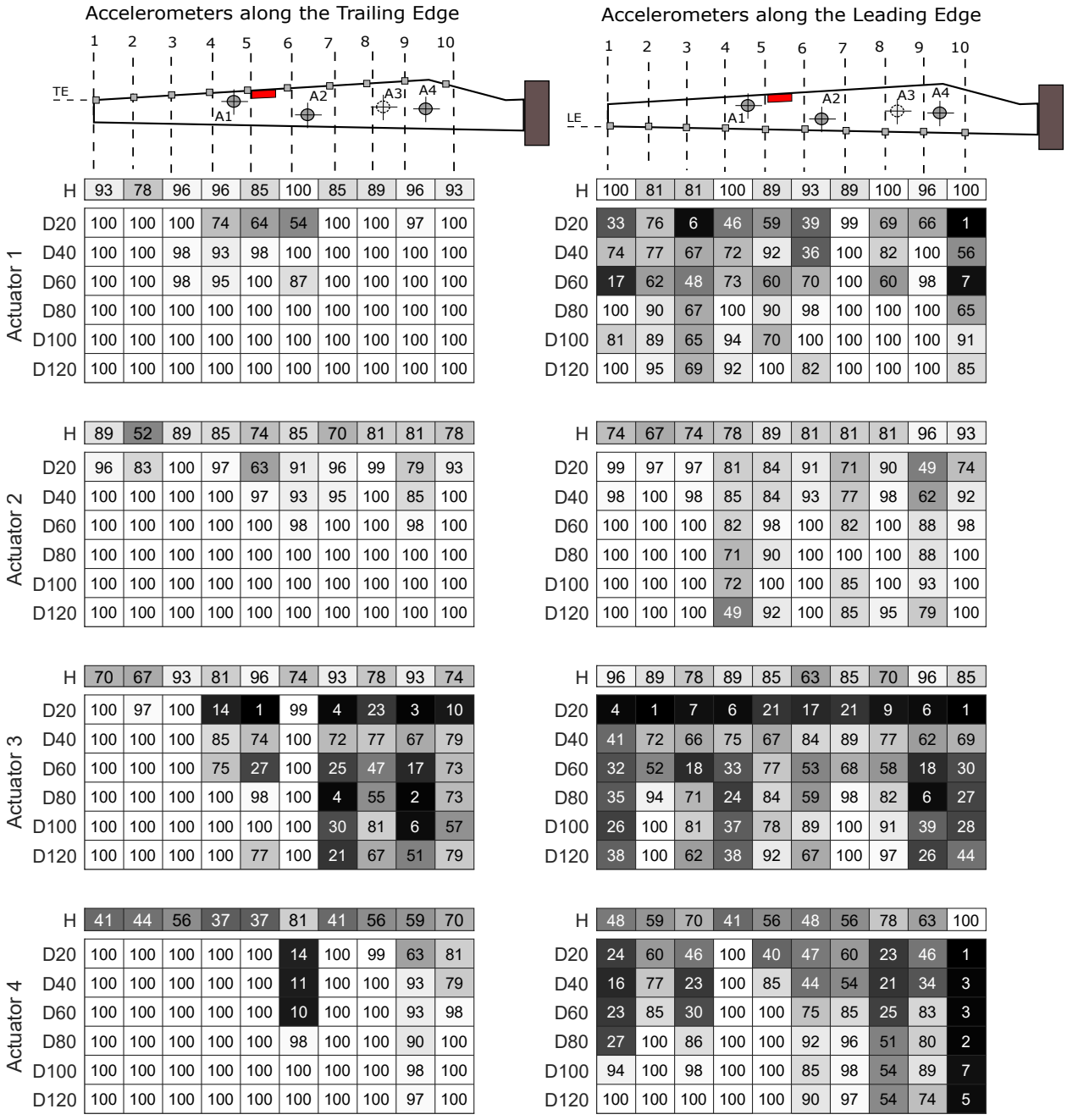

Figure 9: Percentage of correct classification rates for undamaged and different damaged observations (true negatives and true positives) in the accelerometers along the Trailing and Leading Edge. Threshold at risk of false alarm probability equal to $\alpha = 0.01$. The FV dimension is $p = 5$. The number of observations for each scenario are defined in Table 1.

the state of the blade and it would be difficult or uncertain to decide whether the blade was undamaged or damaged. In this section, it is studied how sensitive, the selected feature was for monitoring the progression of the damage. The intend of using the median value of the damage indices for each damage scenario is to

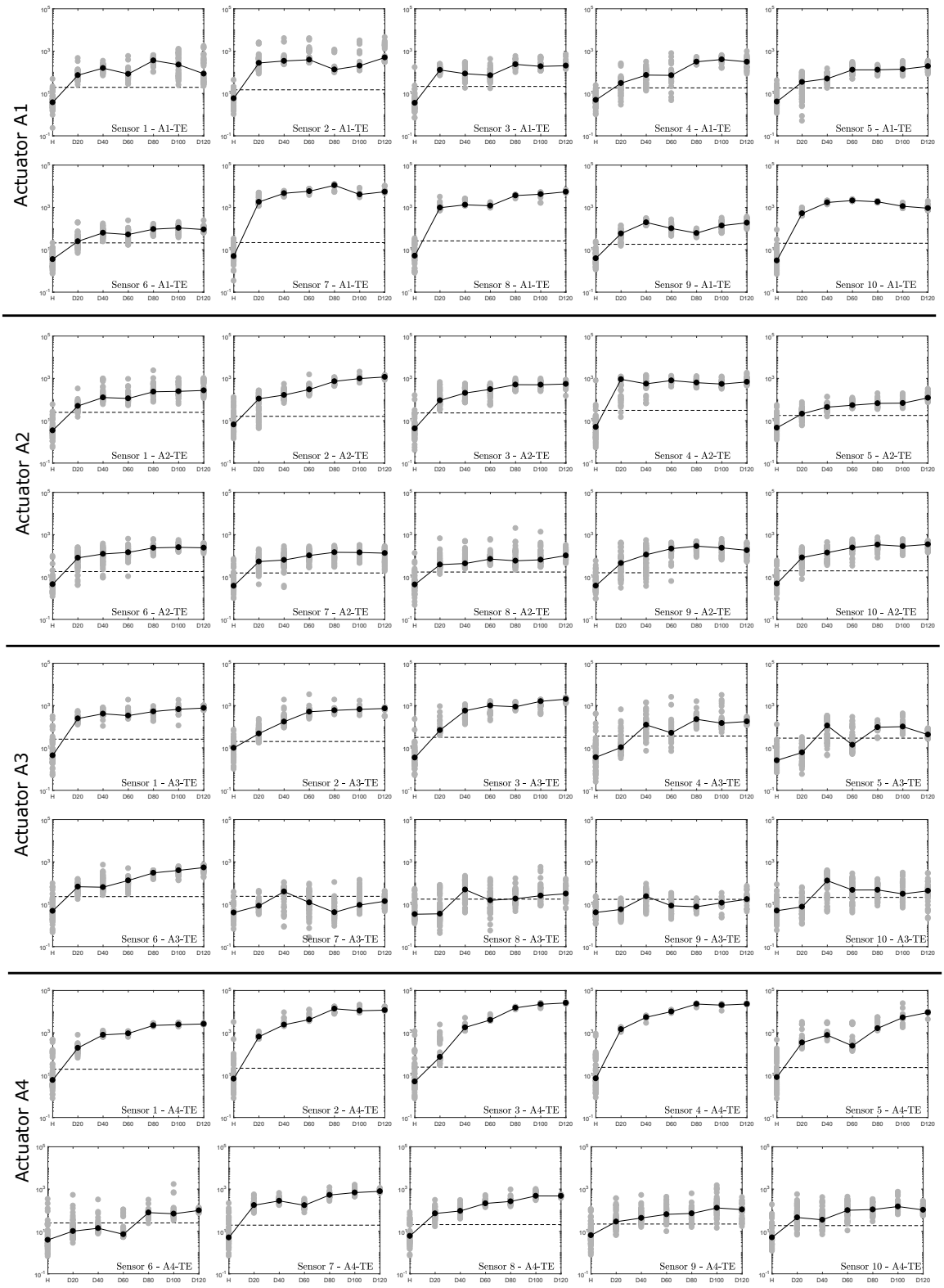

Figure 10: Trend of the damage indices by the damage growth for accelerometers 1 to 10 in the Trailing Edge (TE) by the actuation at location A1, A2, A3 and A4, respectively. The damage index observations for each damage severity (●) and the median of the damage indices of all observations for each damage severity (●). The dashed line is the threshold calculated by a risk of false alarm probability equal to $\alpha = 0.01$.

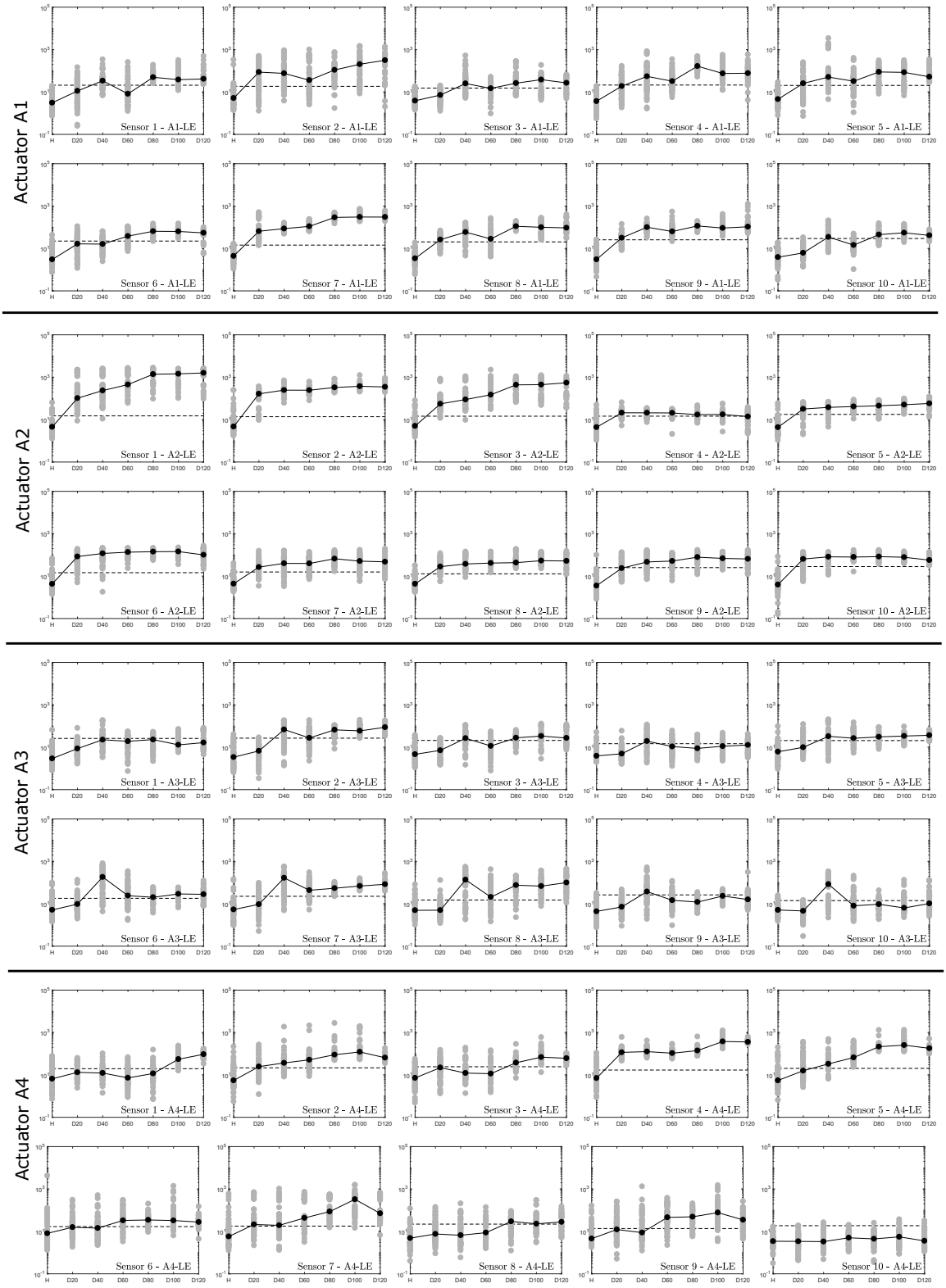

Figure 11: Trend of the damage indices by the damage growth for sensors 1 to 10 in the Leading Edge (LE) by the actuation at location A1, A2, A3 and A4 respectively. The damage index observations for each damage severity (●) and the median of the damage indices of all observations for each damage severity (●). The dashed line is the threshold calculated by a risk of false alarm probability equal to $\alpha = 0.01$.

identify if the amount of damage (after it has occurred) got stabilized or continues to grow. It is believed that this is a valuable information for the decision maker, as a progressing damage may require higher attention, and perhaps, some immediate action from the decision maker. In this study, it is not claimed any robust indicator of damage development but rather provide an evidence that even the data from a single sensor contains some information regarding damage progression. Fig. 10 and 11 contain the damage indices of the observations for each damage size measured by each accelerometer along the TE and LE respectively when the blade was excited at the different actuator locations. Fig. 10 and 11 also contain the median value of the damage indices for each blade state (i.e. undamaged and different damaged sizes of the blade) to visualize the trend of the damage progression. Similarly to the previous section, it was clearly observed that when the methodology was evaluated by measurements from accelerometers along the LE, it did not provide a clear monotonic increasing trend of the damage indices and hence the damage progression was not successfully tracked. However, the results demonstrated a monotonic increasing function for the majority of the accelerometers in the trailing edge when the actuation was at location A1 and A2. These locations also achieved a reasonable high percentage of true negatives and true positives. Therefore, it could be observed that the damage indices increased along with the size of the damage. However, not all accelerometers were able to detect the damage progression for an excitation in the location A3. This was expected as the percentage of the true positives achieved by accelerometers when the blade was excited on A3 was not high and this was also reflected in the damage progression analysis. It can be observed that the accelerometers, after the damage, from the actuator to damage direction, tracked better the damage progression by means of an increment of the damage indices. For example, in the accelerometers in the TE; when the excitation was in the location A2 and A4, the accelerometers 1, 2, 3 provided a good tracking of the damage progression and when the actuation was in the location A1, the accelerometers 7, 8 were also able to track the damage progression. However, in the cases when the percentage of true negatives and true positives was not high, it was difficult to draw a conclusion about the damage detection. Although, the damage was not successfully detected by means of high percentage of the classification rate for some accelerometer's locations, the damage indices still increased with the severity of the damage.

5. Conclusions

The work presented herein introduced an experimental study for damage detection and its monitoring in a large wind turbine blade by using a single accelerometer and actuator through a data-driven SHM methodology. The methodology presented considers a simple nonparametric technique for data compression and information extraction. The vibration responses used as input in the methodology were obtained by an active VSHM system that utilizes an electromechanical actuator (automatic hammer) and an array of accelerometers. First, the performance of the methodology was studied by a fixed accelerometer, a fixed actuator and a fixed damage location to study the effect of the FV dimensions in the damage detection. And secondly, the performance of the methodology at a fixed damage location, at given single actuator locations,

to study the response of each accelerometer on the blade independently.

The results demonstrated that, when the methodology was applied to the signals from the accelerometers along the trailing edge, the damage of the trailing edge was detected with higher confidence compared to when the signals from the leading edge accelerometers were used. In addition, when the excitation was applied at locations A1 and A2, which are the closest to the damaged area and to the tip of the blade, the true negative and true positive rates were high for the majority of the accelerometers along the trailing edge. However, for the actuator locations A3 and A4, the true negative and true positive rates decreased significantly, which made the damage detection poor for some accelerometer locations. This demonstrated that the position of the accelerometer/actuator plays an important role in the damage detection. Therefore, for a damage in the TE, the best locations for the accelerometers are also along the trailing edge. In addition, based on the comparison of the methodology's performance for all the accelerometer locations (leading and trailing edge), a rough information about the damage location can be obtained. The highest percentage of true negatives and true positives was achieved in accelerometers in the trailing edge, which is the edge where the damage is located. The progression of the damage was also assessed by tracking the value of the damage indices. This was assessed by the assumption that an increment in the size of the damage will increase the damage index. The results demonstrated a monotonic increasing function for most of the accelerometers in the trailing edge when the actuation was in the location A1 or A2. These locations also achieved a reasonably high percentage of true negatives and true positives. However, for cases when the percentage of true negatives and true positives was not high, it was difficult to draw a conclusion about the damage detection. However, it could be observed that the damage indices increased with the size of the damage. Although, the damage was not successfully detected by means of high percentage of true negatives and true positives for some accelerometer's locations, the damage indices still increased with the severity of the damage. To conclude, this study demonstrated the potential of a data-driven SHM methodology for a reasonable damage diagnosis in a large wind turbine blade when only one accelerometer and one actuation location was considered.

Acknowledgements

The work was partly supported by EUDP (Danish Energy Technology Development and Demonstration Programme), grant number 64011-0084 'Predictive Structure Health Monitoring of Wind Turbines'.
The authors would like to thank DTU Wind Energy for giving access to the test object and research engineer Per Hørlyk Nielsen for his great assistance in setting up and conducting the experiment.

References

[1] C. C. Ciang, J. R. Lee, H. J. Bang, Structural health monitoring for a wind turbine system: a review of damage detection methods, Measurement Science and Technology 19 (12) (2008) 122001.

[2] C. R. Farrar, K. Worden, An introduction to structural health monitoring, Philosophical Transactions of the Royal Society of London A: Mathematical, Physical and Engineering Sciences 365 (1851) (2007) 303–315.

[3] K. Worden, C. R. Farrar, G. Manson, G. Park, The fundamental axioms of structural health monitoring, in: Proceedings of the Royal Society of London A: Mathematical, Physical and Engineering Sciences, Vol. 463, The Royal Society, 2007, pp. 1639–1664.

[4] K. Maes, A. Iliopoulos, W. Weijtjens, C. Devriendt, G. Lombaert, Dynamic strain estimation for fatigue assessment of an offshore monopile wind turbine using filtering and modal expansion algorithms, Mechanical Systems and Signal Processing 76 (2016) 592–611.

[5] L. D. Avendaño-Valencia, E. N. Chatzi, M. D. Spiridonakos, Non-stationary random coefficient models for vibration-based SHM in structures influenced by strong operational and environmental variability, in: Proceedings of the 10th International Workshop on Structural Health Monitoring (IWSHM 2015), Stanford, CA, USA, 2015, pp. 1–3.

[6] B. C. Love, Comparing supervised and unsupervised category learning, Psychonomic bulletin & review 9 (4) (2002) 829–835.

[7] S. D. Fassois, F. P. Kopsaftopoulos, Statistical time series methods for vibration based structural health monitoring, Springer, 2013.

[8] H. Sohn, J. A. Czarnecki, C. R. Farrar, Structural health monitoring using statistical process control, Journal of Structural Engineering 126 (11) (2000) 1356–1363.

[9] A.-M. Yan, G. Kerschen, P. De Boe, J.-C. Golinval, Structural damage diagnosis under varying environmental conditions—part i: a linear analysis, Mechanical Systems and Signal Processing 19 (4) (2005) 847–864.

[10] A.-M. Yan, G. Kerschen, P. De Boe, J.-C. Golinval, Structural damage diagnosis under varying environmental conditions—part ii: local pca for non-linear cases, Mechanical Systems and Signal Processing 19 (4) (2005) 865–880.

[11] I. T. Jolliffe, Principal component analysis, Vol. 487, Springer-Verlag New York, 1986.

[12] M. Johnson, Waveform based clustering and classification of AE transients in composite laminates using principal component analysis, NDT & E International 35 (6) (2002) 367–376.

[13] A. G. González, S. Fassois, A supervised vibration-based statistical methodology for damage detection under varying environmental conditions & its laboratory assessment with a scale wind turbine blade, Journal of Sound and Vibration 366 (2016) 484–500.

[14] N. Golyandina, V. Nekrutkin, A. A. Zhigljavsky, Analysis of time series structure: SSA and related techniques, CRC Press, 2010.

[15] C.-H. Loh, M.-H. Tseng, S.-H. Chao, Structural damage assessment using output-only measurement: Localization and quantification, in: ASME 2013 Conference on Smart Materials, Adaptive Structures and Intelligent Systems, American Society of Mechanical Engineers, 2013, pp. V002T05A001–V002T05A001.

[16] H. Al-Bugharbee, I. Trendafilova, A fault diagnosis methodology for rolling element bearings based on advanced signal pretreatment and autoregressive modelling, Journal of Sound and Vibration 369 (2016) 246–265.

[17] M. A. de Oliveira, J. Vieira Filho, V. Lopes Jr, D. J. Inman, A new approach for structural damage detection exploring the singular spectrum analysis, Journal of Intelligent Material Systems and Structures 28 (9) (2017) 1160–1174.

[18] J. Zabalza, J. Ren, J. Zheng, J. Han, H. Zhao, S. Li, S. Marshall, Novel two-dimensional singular spectrum analysis for effective feature extraction and data classification in hyperspectral imaging, IEEE Transactions on Geoscience and Remote Sensing 53 (8) (2015) 4418–4433.

[19] D. Garcia, I. Trendafilova, Study on singular spectrum analysis as a data-driven technique for damage diagnosis. Comparison between time and frequency domain., in: MATEC Web of Conferences, Vol. 148, EDP Sciences, 2018, p. 14003.

[20] D. Tcherniak, L. L. Mølgaard, Active vibration-based structural health monitoring system for wind turbine blade: Demonstration on an operating Vestas V27 wind turbine, Structural Health Monitoring 16 (5) (2017) 536–550.

[21] T. Bull, M. D. Ulriksen, D. Tcherniak, The effect of environmental and operational variabilities on damage detection in wind turbine blades, in: Proceedings of the 9th European Workshop on Structural Health Monitoring, 2018.

[22] M. Friswell, J. Penny, Is damage location using vibration measurements practical?, in: Proceedings of EUROMECH 365 international workshop: DAMAS, Vol. 97, 1997.

[23] G. C. Larsen, P. Berring, D. Tcherniak, P. H. Nielsen, K. Branner, Effect of a damage to modal parameters of a wind turbine blade, in: EWSHM-7th European Workshop on Structural Health Monitoring, 2014.

[24] M. A. Eder, K. Branner, P. Berring, F. Belloni, H. S. Toft, J. D. Sørensen, A. Corre, T. Lindby, A. Quispitupa, T. K. Petersen, Experimental blade research: Phase 2.

[25] D. Garcia, D. Tcherniak, K. Branner, Virtual prototyping of an actuator-based structural health monitoring system of wind turbine blades, in: 28th International Conference on Noise and Vibration Engineering, 2018.

[26] D. Tcherniak, L. L. Mølgaard, Vibration-based shm system: Application to wind turbine blades, in: Journal of Physics: Conference Series, Vol. 628, IOP Publishing, 2015, p. 012072.

[27] M. Ghil, M. Allen, M. Dettinger, K. Ide, D. Kondrashov, M. Mann, A. W. Robertson, A. Saunders, Y. Tian, F. Varadi, et al., Advanced spectral methods for climatic time series, Reviews of Geophysics 40 (1) (2002) 1003.

[28] D. Garcia, I. Trendafilova, A multivariate data analysis approach towards vibration analysis and vibration-based damage assessment: Application for delamination detection in a composite beam, Journal of Sound and Vibration 333 (25) (2014) 7036–7050.

[29] H. Sohn, D. W. Allen, K. Worden, C. R. Farrar, Statistical damage classification using sequential probability ratio tests, Structural Health Monitoring 2 (1) (2003) 57–74.

[30] L. Andrews, Special functions of mathematics for engineers (1998).

[31] M. Nielsen, A. Roczek-Sieradzan, P. H. Nielsen, P. Berring, T. Sieradzan, V. Roudnitski, R. Bitsche, H. W. Knudsen, A. B. Rasmussen, J. J. A. Rasmussen, et al., Full scale test SSP 34 m blade, edgewise loading LTT. Extreme load and PoC_InvE data report.

[32] M. D. Ulriksen, D. Tcherniak, L. Damkilde, Damage detection in an operating Vestas V27 wind turbine blade by use of outlier analysis, in: Environmental, Energy and Structural Monitoring Systems (EESMS), 2015 IEEE Workshop on, IEEE, 2015, pp. 50–55.

[33] M. Zhu, A. Ghodsi, Automatic dimensionality selection from the scree plot via the use of profile likelihood, Computational Statistics & Data Analysis 51 (2) (2006) 918–930.